Ultrafast Carrier Dynamics in Wide Band Gap Mixed-Cation Perovskites: Influence of the Cs Cation

Mahmoud M. Elshanawany, Antonio Gaetano Ricciardulli, Jose J. Jeronimo-Rendon, Michael Saliba, Josef Wachtveitl, and Markus Braun*

Read Online

ACCESS | 📊 Metrics & More | 📖 Article Recommendations | 🆂🅸 Supporting Information

ABSTRACT: Mixed-cation perovskites exhibit outstanding performance as next-generation solar cells and for optoelectronic applications. One pathway to increase the quality and stability of these materials is adding Cs to the A-site of mixed-cation formamidinium/methylammonium in the perovskite $APbX_3$. Here, we use femtosecond transient absorption spectroscopy to study the effect of Cs on the dynamics of a mixed-cation wide band gap bromide-based perovskite. Negligible changes in the optical spectra are observed between the two films, indicating a similar localization of the charge carriers at the band edge. However, adding Cs reduces the non-radiative recombination sites and increases the lifetime of the photogenerated charge carriers in the perovskite film (from 291 to 355 ns). Furthermore, the Cs cation slows down the cooling of hot carriers through an efficient hot-phonon bottleneck, which is observed by increasing the excitation power from 9.7 to 648 $\mu J/cm^2$ [the lifetime of the fast component (τ_1) increases from 0.21 to 0.91 ps]. Understanding the mechanism of charge dynamics in perovskite thin films is critical for the fabrication of high-performance devices.
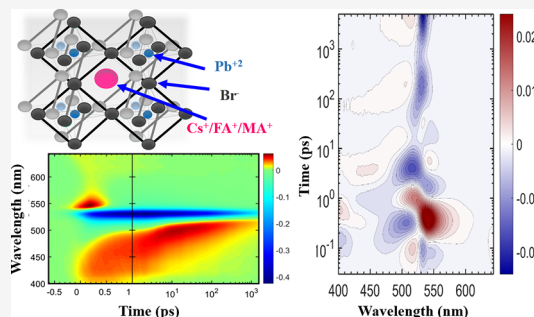
INTRODUCTION

Hybrid organic−inorganic lead halide perovskite solar cells (PSCs) have attracted much attention over the past 10 years as a pre-eminent candidate for the next generation of solar cells (SCs) due to their excellent optoelectronic properties, simple fabrication, and low-cost processing.[1−3] The possibility of changing the cation A, metal B, or halide X in the perovskite structure (ABX_3) opened many opportunities for novel material synthesis with power conversion efficiencies of more than 25%[1,2] using $FAPbI_3$-rich perovskites with a band gap close to 1.5 eV.

A is a monovalent cation such as methylammonium (MA^+), formamidinium (FA^+), or the inorganic cation Cs^+, B is a divalent metal cation such as lead (Pb^{2+}) or tin (Sn^{2+}), and X is a halide anion (Cl^-, Br^-, and I^-). Triple cation PSCs with a Cs/FA/MA mixture at the A-site exhibit promising results toward an efficient and stable SC.[4−8] In addition, Cs/FA/MA perovskites show high efficiencies,[2,9] thermal stability,[10,11] improved stability against humidity,[12,13] increased reproducibility, and decreased trap state formation.[14] Replacing iodide with bromide leads to perovskite materials with increased stability against air, but it is less efficient for single-junction SCs due to its high band gap >1.8 eV.[8,15−17] As wide band gap semiconductors, bromide-based perovskites offer promising possibilities for optoelectronic applications such as sensors, water splitters, light-emitting diodes (LEDs), and multi-junction high-performance SCs.[7,17−20]

Much effort has been made to understand the dynamics of the single-cation perovskite photophysics using ultrafast transient absorption spectroscopy (TAS).[14,21−27] TAS is a powerful technique to visualize carrier excitation, recombination, relaxation, and energy transfer on a subpicosecond time scale.[28−31] Ghosh et al. reported the separation time of the initial photo-excited excitons into free charge carriers (20 fs) by performing a 10 fs resolution experiment,[32] which is followed by charge carrier thermalization (sub-100 fs time range).[32] Polaron formation occurs between 0.3 and 0.7 ps depending on the used cations (0.3 ps in the case of $MAPbBr_3$ and 0.7 ps in $CsPbBr_3$).[33] The time constant for subsequent carrier cooling was determined to be 230 fs for low carrier densities, which is slowed down to 770 fs for higher carrier densities.[25] This behavior is attributed to a hot-phonon bottleneck effect. Later signal decay extending to the nanosecond time scale obeys second-order kinetics due to charge recombination.[21]

Typically, charge carrier extraction in SCs is assisted by electron or hole transport layers. Reducing recombination
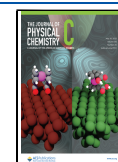
losses before carrier extraction is critical for enhancing the efficiency of perovskite SCs.[34] Recently, some dynamics studies on mixed-cation halide perovskite have been reported.[35−43] However, the role of Cs in FA/MA hybrid perovskite has received less attention so far.

In this work, we used time-resolved spectroscopic techniques [steady-state spectroscopy, time-resolved emission, and ultrafast femtosecond TAS (fs-TAS)] to study the excited-state dynamics of $FA_{0.83}MA_{0.17}PbBr_3$ with or without 5% Cs to elucidate the underlying mechanism and relaxation pathways.

■ EXPERIMENTAL SECTION

The one-step spin-coating method was applied to fabricate thin films of microcrystalline $FA_{0.83}MA_{0.17}PbBr_3$ and $Cs_{0.05}(FA_{0.83}MA_{0.17})_{0.95}PbBr_3$ on a glass substrate as reported elsewhere.[7,44] For the sake of simplicity, we will name these perovskite samples as FA/MA and Cs/FA/MA films in the following.

Materials. The chemicals used to fabricate perovskite films are commercially available from the specified suppliers. N, N-dimethylformamide (DMF), dimethyl sulfoxide (DMSO), and anisole were purchased from Acros Organics. Caesium bromide (CsBr, ultradry (99.998%)) was bought from abcr GmbH. Formamidinium bromide (FABr) and methylammonium bromide (MABr) were purchased from Greatcell solar. Lead bromide ($PbBr_2$) was bought from Tokyo Chemical Industry (TCI) Co.

Preparation of Perovskite Thin Films. The perovskite films of Cs/FA/MA and FA/MA lead bromide were prepared by spin coating via the antisolvent method on glass substrates. First, glass substrates were cleaned in 2% Hellmanex deionized water solution with the assistance of an ultrasonic bath. Subsequently, the substrates were further cleaned with acetone, 2-propanol, and UV ozone treatment for 15 min. The perovskite solution was prepared following a triple cation process.[44] The $FAPbBr_3$ precursor solution was prepared by dissolving FABr and $PbBr_2$ (molar ratio 1:1.1) in anhydrous DMF/DMSO 4:1 (v/v). In contrast, $MAPbBr_3$ solution was prepared by dissolving the precursors, MABr (1 M) and $PbBr_2$ (1.1 M), dissolved in the DMF/DMSO solvent mixture. Furthermore, the double cation perovskite (FA/MA) was prepared by mixing the solutions of $FAPbBr_3$ and $MAPbBr_3$, respectively, with an 83:17 volume ratio. To obtain the triple cation perovskite, 5 vol % solution of the inorganic salt CsBr (1.5 M) in DMSO was added to the double cation perovskite precursor.[8] Finally, 100 μL of the perovskite solution was deposited using spin coating in one step (30 s at 3000 rpm and 2000 rpm/s). Ten seconds before the end of the process, 200 μL of anisole, an antisolvent, was poured on the spinning substrate. Then, the substrates were annealed at 100 °C for 45 min. The entire process was carried out in a nitrogen-filled glovebox. As shown in Figures S1 and S2, the X-ray diffraction (XRD) spectra and scanning electron microscopy (SEM) images of both films exhibit high crystallinity and morphology of these films, respectively.

Steady-State Spectroscopy. Absorption spectra of the spin-coated films on a glass substrate (thickness 1 mm) were recorded with the SPECORD S600 UV/vis spectrophotometer (Analytik Jena, Jena, Germany). PL spectra were collected with an FP-8500 spectrofluorometer (Jasco, Groß-Umstadt, Germany). The excitation wavelength was 362 nm with a bandwidth of 5 nm. For additional spectral cleaning, we applied a UV band-pass filter between 280 and 370 nm (UG11, Schott Glas) for the excitation path and a long pass filter at 360 nm (WG360, Schott Glas) for the emission path, respectively. The PMT voltage was set to 650 V. The wavelength-dependent instrument sensitivity and the baseline were corrected routinely. All measurements were performed at room temperature under ambient conditions.

Time-Correlated Single-Photon Counting. We used our home-built time-correlated single-photon counting (TCSPC) setup with a counting card for recording time-resolved PL data.[45,46] Briefly, the thin films were excited using a mode-locked titanium-doped sapphire (Ti/Sa) laser (Tsunami 3941-X3BB, Spectra-Physics, Darmstadt, Germany), which was pumped by a 8 W continuous wave diode pumped solid-state laser (Millennia eV, Spectra-Physics, 532 nm). The Ti/Sa laser allowed the tuning of the excitation wavelength to 775 nm with a pulse width of 100 fs at a repetition rate of 80 MHz. The acoustooptic modulator assisted to reduce the repetition rate to 160 kHz. The excitation wavelength of 387 nm was obtained by second harmonic generation (SHG) in a BBO crystal (frequency doubler and pulse selector, model 3980, Spectra-Physics). We used excitation filters (UG11, BG38, Schott AG, Mainz, Germany) to block remaining fundamental light from the SHG excitation pulses. The instrument response function (IRF, FWHM 200 ps) was obtained without emission filters using an empty glass substrate as a scattering sample. A photomultiplier tube (PMT, PMA-C 182-M, PicoQuant, Berlin, Germany) and a TimeHarp 260 PICO Single PCIe card (PicoQuant) were used for single-photon detection (channel width adjusted to 400 ps). Long-pass filters at 400 and 470 nm were inserted routinely to block stray light from the excitation pulses for both samples.

Femtosecond Transient Absorption Spectroscopy Measurements. We used fs-TAS to investigate the ultrafast excited-state dynamics and the recombination processes in the mixed cation perovskite systems using a home-built pump−probe setup.[47] Briefly, the excitation pump pulses were applied at a central wavelength of 387 nm (SHG of the laser fundamental). The pulsed laser system was running at 775 nm central wavelength and 1 kHz repetition rate (Clark-MXR, Dexter, MI, USA) with a pulse duration of 150 fs. The excitation power was adjusted between 9.7 and 648 μJ cm^{-2} at the sample position. The probe white light covering a spectral range of 400−645 nm was generated by focusing a part of the laser fundamental onto a 5 mm thick calcium fluoride crystal. The white light was transmitted through the sample and subsequently detected via an HR320 spectrograph (Horiba, Kyoto, Japan). The detection system consists of a signal-processing chip (S8865-128) with 128 channel photodiode arrays (PDA), a C9118 driver circuit (Hamamatsu Photonics), and a data acquisition card that digitizes the analogue PDA signals at 16 bits (National Instruments, NI6120). The sample was continuously moved in the plane perpendicular to the direction of probe pulse propagation. The measurements for both samples were performed at room temperature under ambient conditions.

Data evaluation of the transient absorption data was performed by the software package Optimus.[48] The data sets were fitted via a GLA to a multiexponential model with decay times τ_i and related decay-associated spectra (DAS). Additionally, the data sets were converted by a model-free method, the so-called lifetime density analysis (LDA), which is a numerical variant of the Laplace transformation.
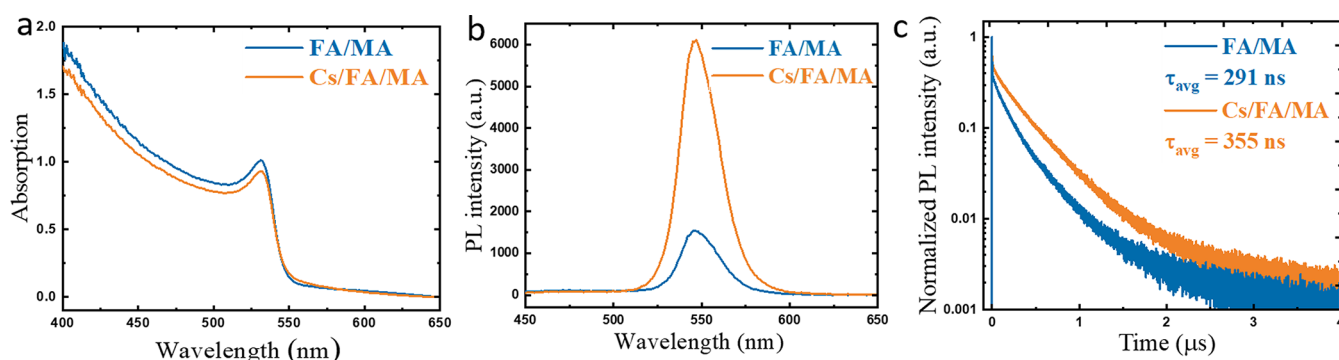
Figure 1. (a) Steady-state absorption, (b) steady-state photoluminescence (PL) spectra with optical excitation at 362 nm, and (c) time-resolved (PL) decay with optical excitation at 387 nm of FA/MA (blue) and Cs/FA/MA (orange) thin films deposited on glass substrates at room temperature.
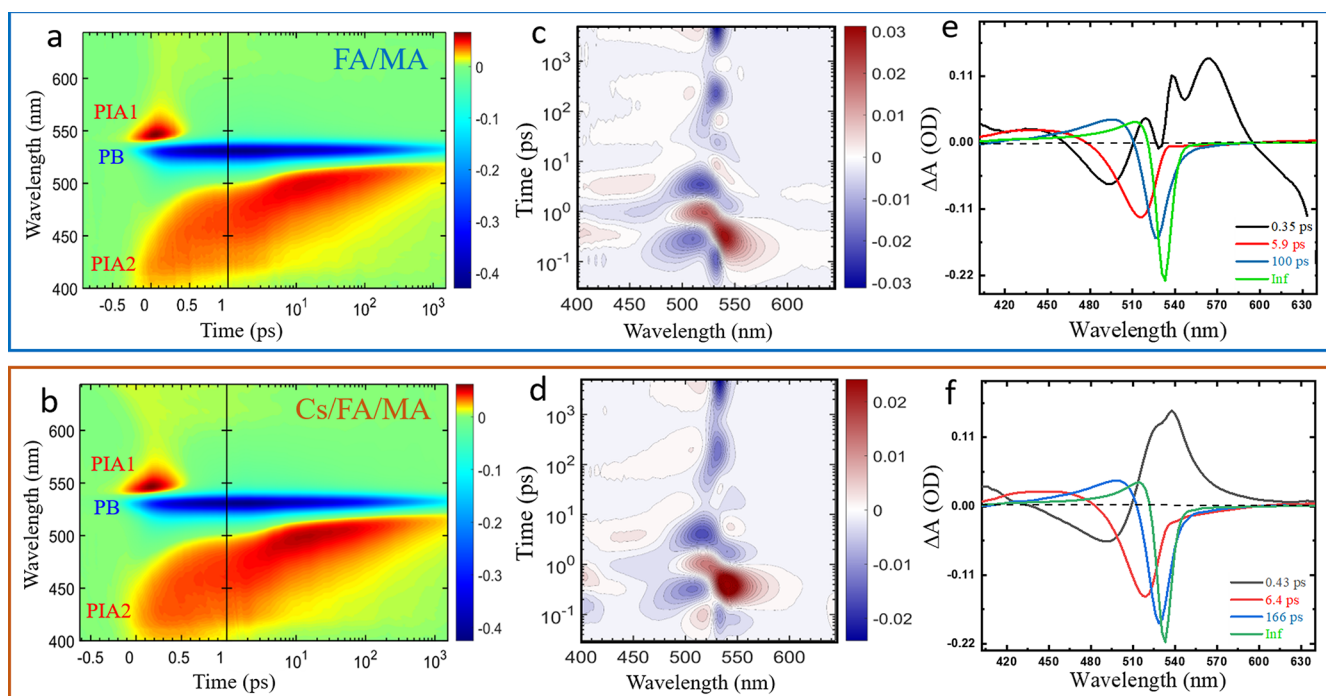

Figure 2. (a,b) Wavelength and time-dependent TA map of FA/MA (upper panel) and Cs/FA/MA (lower panel) films, (c,d) corresponding lifetime density maps (LDM) obtained from the lifetime distribution analysis of the TA data displayed in (a,b). (e,f) Decay-associated spectra (DAS) from a global lifetime analysis (GLA) to a sequential model with three exponential decay components and a remaining spectrum at the end of the experimental time window (inf). Both films were excited with a laser pulse of 387 nm and a fluence of 324 μJ cm^{-2}.

■ RESULTS AND DISCUSSION

Here, we present the optical properties of the spin-coated FA$_{0.83}$MA$_{0.17}$PbBr$_3$ thin films with and without 5% Cs on a glass substrate. As shown in Figure 1a, the absorption spectra of both samples are identical. Both compositions show a broad continuum with a sharp absorption peak at 532 nm (2.33 eV), the excitonic absorption of the materials. The emission spectra of both films have a maximum at 546 nm (2.2 eV), but the addition of Cs enhances the PL intensity by a factor of four (shown in Figure 1b), which indicates a reduction of the non-radiative recombination sites in the perovskite film. Moreover, we investigated the dynamics of the charge carrier relaxation by time-resolved PL with the TCSPC method. As shown in Figure 1c, the Cs/FA/MA film has a longer average lifetime (355 ns) than the FA/MA film (291 ns), which is also in agreement with fewer non-radiative recombination channels and a reduced trap density in the triple cation sample.

A closer look is taken at the photophysics of both thin films using fs-TAS after photoexcitation at 387 nm and in a probing spectral region between 400 and 645 nm. Both samples showed transient spectral features similar to those reported in previously published work.[36,49]

The TAS results of both thin films excited with an excitation density of 324 μJ/cm^2 are shown in Figure 2. The wavelength and time-dependent TA maps are shown in Figure 2a for the FA/MA film and Figure 2b for the Cs/FA/MA film. In both samples, the photobleaching (PB) of the excitonic ground-state absorption centered at 532 nm (2.33 eV) is observed in accordance with the steady-state absorption spectrum. Slightly red-shifted to this signal a photoinduced absorption (PIA1) signal is observed at 539 nm (2.30 eV) for early delay times. This is related to a transient Stark shift of the excitonic transition due to charge carriers, after exciton dissociation. In the spectral range between 400 and 520 nm, a photoinduced
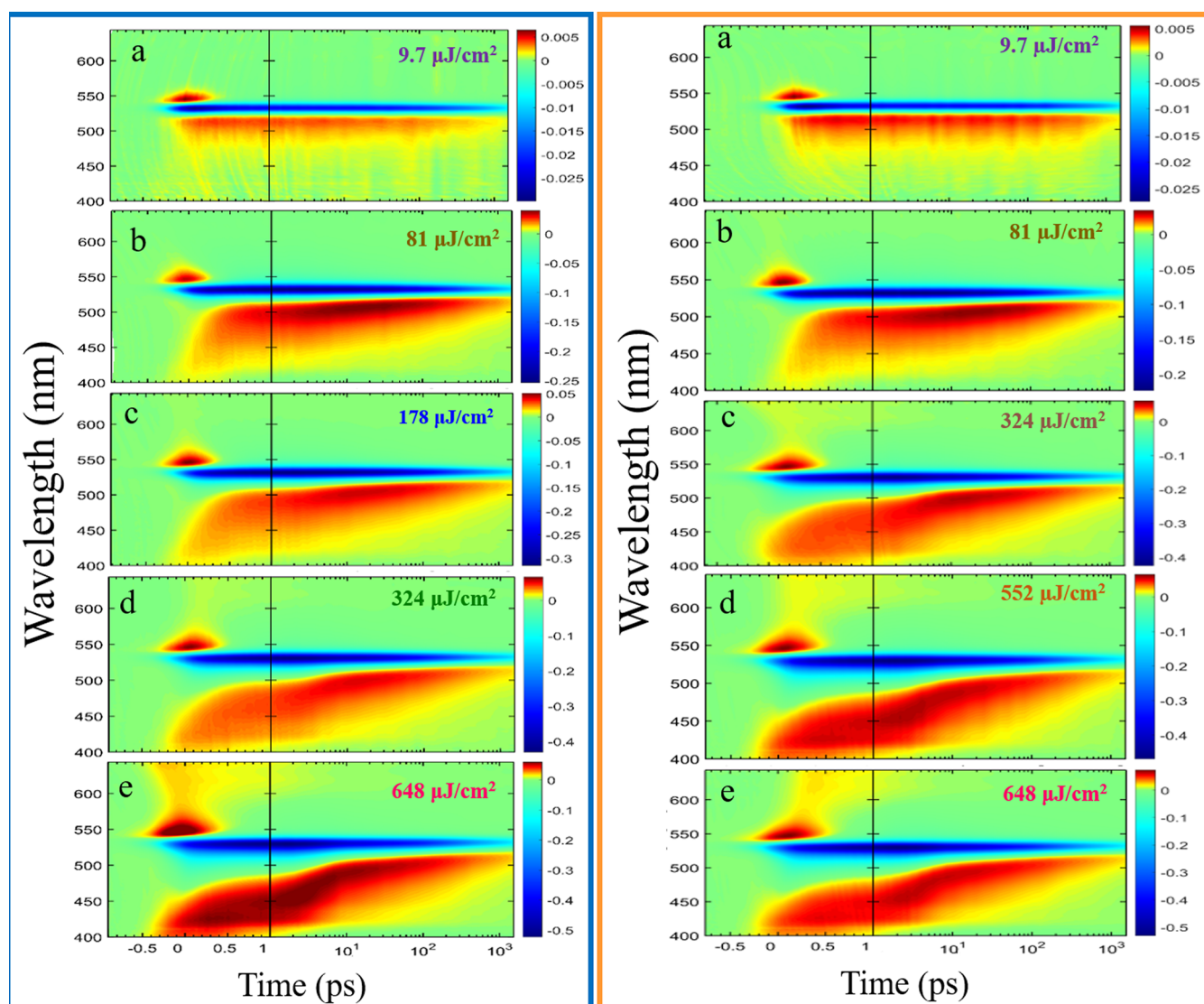
Figure 3. TA measurement on the FA/MA film up to 1.5 ns at (a) 9.7, (b) 81, (c) 178, (d) 324, and (e) 648 $\mu J/cm^2$ for different excitation powers (left panel). TA measurement on the Cs/FA/MA film at (a) 9.7, (b) 81, (c) 324, (d) 552, and (e) 648 $\mu J/cm^2$ for different excitation powers up to 1.5 ns (right panel). Both films were excited by optical pump pulses at 387 nm. A quantitative evaluation of these datasets was done by GLA and is presented in Tables S1 and S2. An evaluation of these data sets by LDA is presented in Figure S7.

absorption (PIA2) signal with a non-exponential dynamic spectral shift is monitored, which can be assigned to the relaxation of free charge carriers. The origin of this signal was first ascribed to intraband transitions,[50] but a recent study, which combined transient absorption with transient reflectance data, attributed this signal to increased sample reflectivity due to a photoinduced change of the refractive index.[25]

The LDMs of both samples are shown in Figure 2c (FA/MA film) and Figure 2d (Cs/FA/MA film) (see also Figure S7 for all powers). The positive LDM signal at 539 nm (PIA1) assigns a decay time of 0.2 ps to the PIA1 signal decay. At a wavelength of 532 nm (PB), the LDM plot shows an extended negative range between 5 ps and 3 ns. This illustrates that the PB signal of the samples decays via non-exponential decay kinetics. In the spectral range between 400 and 520 nm (PIA2), several tilted negative and positive areas are seen in the LDM plot between 1 and 100 ps. This shows that the PIA2 signal decays non-exponentially combined with a transient spectral shift from 400 to 520 nm.

In the following, the transient data set will be parametrized by a set of exponential decay components. This GLA[48] of the transient data yields DAS related to three lifetimes, and an infinity lifetime accounts for the transient spectrum at the end of our experimental time window [Figure 2e (FA/MA film) and Figure 2f (Cs/FA/MA film)]. The long-lived positive signal (PIA 2) in the region from 400 to 520 nm shows a dynamic red shift, which is assigned to the cooling of free charge carriers. The negative PB signal at 532 nm is assigned to the band-filling effect.[21] The stimulated emission and PB are possibly overlapped in the same transient feature. In the region from 540 to 580 nm, there is a positive feature (PIA1), below the band gap energy only at short delay times (<1 ps). It was also observed in single-cation perovskites such as $MAPbI_3$ and was associated with band gap renormalization (BGR) and transient electroabsorption (Stark effect).[25,36,49−51]

By performing experiments with different excitation power densities in both films, a clear pump power dependence is seen (Figure 3). For high pump powers, we observe a strong blue shift (up to 420 nm) and a broadening of the PIA2 signal at

early delay times, which red-shifts for longer delay times to 520 nm and becomes spectrally narrow. However, for very low pump power, the PIA2 signal appears at early delay times at 520 nm and remains spectrally unchanged also for longer delay times. This indicates that the PIA2 signal is a sensitive indicator for the density and thermal distribution of charge carriers in the thin film.[52] In the FA/MA film, by increasing the power from 9.7 to 648 $\mu J/cm^2$, the slowest carrier relaxation time (τ_3) decreases from 500 to 85 ps, respectively [Figure 3 and Table S1 (Supporting Information)]. The excitation power dependence is directly correlated with the exciton density in the sample. In the Cs/FA/MA film, by increasing the power from 9.7 to 648 $\mu J/cm^2$, the carrier relaxation time (τ_3) decreases from 905 to 124 ps, and the cooling process of the fast component (τ_1) is directly affected by the phonon bottleneck, which slows down the cooling of charge carriers with increasing carrier density.[22,25,26] This phenomenon is observed as well in the FA/MA film with shorter lifetimes (see Figure 3 and Table S2).

Therefore, the fast component τ_1 is compatible with polaron formation.[33] In the case of Cs, increasing the excitation power delays the polaron formation from 0.21 to 0.91 ps; however, in the case of absence of Cs, it delays the polaron formation from 0.2 to 0.84 ps. This excitation density-dependent slowdown in the polaron formation time (τ_1) together with the increase in the decay rate (τ_2 and τ_3) is an indication for the phonon bottleneck.[22] For the perovskite film with an addition of 5% Cs, this effect is slightly enhanced.

Considering the striking linearity of ΔA^{-1} as a function of time for the PB signal (532 nm) for all excitation densities, we could conclude that the recombination mechanism occurs via second-order kinetics. This non-exponential mechanism is approximated in the GLA mainly by the second (τ_2) and third time constant (τ_3) (see Supporting Information, Figures S4 and S6).[21] The fourth time constant (τ_4) for the slowest component, which does not decay in our experimental time window (1.5 ns), is likely due to non-geminate recombination. For a stable fitting process of the data sets, it was set to infinity value.

In a former study, adding 5% of Cs to the perovskite material enabled a relative improvement of 17% in power conversion efficiency (PCE) (16.3 to 19.2%).[7] The present study shows that the main characteristics of ultrafast charge carrier dynamics exhibit only slight changes between the perovskite material with and without addition of Cs. However, the higher fluorescence signal is a clear indication for reduced trap state density. Our observation of the increase in the fluorescence lifetime from 291 to 355 ns after addition of 5% Cs to the perovskite corresponds to a relative increase in the lifetime of 18%. This coincides with the improvement in device performance, mentioned above. This unusual long fluorescence lifetime in the microsecond time range monitors the diffusion of screened charge carriers (polarons) in the perovskite film. If this perovskite material is incorporated in a photovoltaic device between hole- or electron-extracting layers in a typical sandwich geometry, the enlarged charge carrier lifetime would directly improve device performance. The incorporation of a small amount of non-polar Cs cation does not change the polar surrounding dominated by polar MA and FA cations in the perovskite lattice, but obviously the third cation allows a relaxed formation of the perovskite crystal lattice with less traps and therefore better device performance.

A similar observation was reported[36] for photovoltaic devices based on lead halides with a chloride/iodide mixture and a Cs/FA mixture on the A-site. Here, the introduction of polar MA as the third cation type resulted in a more defect-tolerant material with an increased fluorescence intensity and lifetime, which was explained by a reduction of trap-assisted recombination.

■ CONCLUSIONS

In summary, we compared the excited-state properties of FA/MA and Cs/FA/MA mixture perovskite films using fs-TAS upon photoexcitation at 3.2 eV in the visible region (~1.9−3.1 eV) to identify the role of Cs in carrier recombination paths. Adding 5% of Cs showed significant features in their photophysics. The steady-state spectra did not show any apparent change between the two materials, indicating a similar degree of localization of the charge carriers at the band edge (2.33 eV). Moreover, the addition of Cs reduced trap density and terminated non-radiative recombination channels as well as increased the average lifetime of the photogenerated charge carriers from 291 to 355 ns. In the Cs/FA/MA film, we observed the enhancement in the efficient hot-phonon bottleneck due to the large mass and small ionic radius of Cs. Our study suggests that triple-cation lead bromide perovskites will be an exciting target materials for designing photoconversion systems that use slow carrier relaxation for high-efficiency solar energy conversion.

■ ASSOCIATED CONTENT

ⓢ Supporting Information

The Supporting Information is available free of charge at https://pubs.acs.org/doi/10.1021/acs.jpcc.2c02682.

XRD spectra; SEM images; kinetic profiles; results from global fitting; time constants; and lifetime density maps of $FA_{0.83}MA_{0.17}PbBr_3$ and $Cs_{0.05}(FA_{0.83}MA_{0.17})_{0.95}PbBr_3$ thin films on glass (PDF)

■ AUTHOR INFORMATION

Corresponding Author

Markus Braun — *Institute of Physical and Theoretical Chemistry, Goethe University, Frankfurt am Main 60438, Germany;* ⓘ orcid.org/0000-0002-7891-6954; Email: braun@theochem.uni-frankfurt.de

Authors

Mahmoud M. Elshanawany — *Institute of Physical and Theoretical Chemistry, Goethe University, Frankfurt am Main 60438, Germany;* ⓘ orcid.org/0000-0001-9013-1263

Antonio Gaetano Ricciardulli — *Institute of Materials Science, Technische Universität Darmstadt, Darmstadt 64289, Germany;* ⓘ orcid.org/0000-0003-2688-9912

Jose J. Jeronimo-Rendon — *Institute of Photovoltaics (ipv), University of Stuttgart, Stuttgart 70569, Germany*

Michael Saliba — *Institute of Photovoltaics (ipv), University of Stuttgart, Stuttgart 70569, Germany; Helmholtz Young Investigator Group FRONTRUNNER, Forschungszentrum Jülich, Jülich 52428, Germany;* ⓘ orcid.org/0000-0002-6818-9781

Josef Wachtveitl — *Institute of Physical and Theoretical Chemistry, Goethe University, Frankfurt am Main 60438, Germany;* ⓘ orcid.org/0000-0002-8496-8240

Complete contact information is available at:

Notes

The authors declare no competing financial interest.

REFERENCES

(1) National Renewable Energy Laboratory. Best Research-Cell Efficiencies. 2020, https://www.nrel.gov/pv/cell-efficiency.html.

(2) Kojima, A.; Teshima, K.; Shirai, Y.; Miyasaka, T. Organometal Halide Perovskites as Visible-Light Sensitizers for Photovoltaic Cells. *J. Am. Chem. Soc.* 2009, 131, 6050−6051.

(3) Gil-Escrig, L.; Dreessen, C.; Palazon, F.; Hawash, Z.; Moons, E.; Albrecht, S.; Sessolo, M.; Bolink, H. J. Efficient Wide-Bandgap Mixed-Cation and Mixed-Halide Perovskite Solar Cells by Vacuum Deposition. *ACS Energy Lett.* 2021, 6, 827−836.

(4) Jung, E. H.; Jeon, N. J.; Park, E. Y.; Moon, C. S.; Shin, T. J.; Yang, T.-Y.; Noh, J. H.; Seo, J. Efficient, Stable and Scalable Perovskite Solar Cells Using Poly(3-Hexylthiophene). *Nature* 2019, 567, 511−515.

(5) Jiang, Q.; Zhao, Y.; Zhang, X.; Yang, X.; Chen, Y.; Chu, Z.; Ye, Q.; Li, X.; Yin, Z.; You, J. Surface Passivation of Perovskite Film for Efficient Solar Cells. *Nat. Photonics* 2019, 13, 460−466.

(6) Zheng, X.; Hou, Y.; Bao, C.; Yin, J.; Yuan, F.; Huang, Z.; Song, K.; Liu, J.; Troughton, J.; Gasparini, N.; Zhou, C.; Lin, Y.; Xue, D.-J.; Chen, B.; Johnston, A. K.; Wei, N.; Hedhili, M. N.; Wei, M.; Alsalloum, A. Y.; Maity, P.; Turedi, B.; Yang, C.; Baran, D.; Anthopoulos, T. D.; Han, Y.; Lu, Z.-H.; Mohammed, O. F.; Gao, F.; Sargent, E. H.; Bakr, O. M. Managing Grains and Interfaces via Ligand Anchoring Enables 22.3%-Efficiency Inverted Perovskite Solar Cells. *Nat. Energy* 2020, 5, 131−140.

(7) Saliba, M.; Matsui, T.; Seo, J.-Y.; Domanski, K.; Correa-Baena, J.-P.; Nazeeruddin, M. K.; Zakeeruddin, S. M.; Tress, W.; Abate, A.; Hagfeldt, A.; Grätzel, M. Cesium-Containing Triple Cation Perovskite Solar Cells: Improved Stability, Reproducibility and High Efficiency. *Energy Environ. Sci.* 2016, 9, 1989−1997.

(8) Ferdowsi, P.; Ochoa-Martinez, E.; Steiner, U.; Saliba, M. One-Step Solvent-Free Mechanochemical Incorporation of Insoluble Cesium Salt into Perovskites for Wide Band-Gap Solar Cells. *Chem. Mater.* 2021, 33, 3971−3979.

(9) Lee, M. M.; Teuscher, J.; Miyasaka, T.; Murakami, T. N.; Snaith, H. J. Efficient Hybrid Solar Cells Based on Meso-Superstructured Organometal Halide Perovskites. *Science* 2012, 338, 643−647.

(10) Conings, B.; Drijkoningen, J.; Gauquelin, N.; Babayigit, A.; D'Haen, J.; D'Olieslaeger, L.; Ethirajan, A.; Verbeeck, J.; Manca, J.; Mosconi, E.; Angelis, F. D.; Boyen, H.-G. Intrinsic Thermal Instability of Methylammonium Lead Trihalide Perovskite. *Adv. Energy Mater.* 2015, 5, 1500477.

(11) Misra, R. K.; Aharon, S.; Li, B.; Mogilyansky, D.; Visoly-Fisher, I.; Etgar, L.; Katz, E. A. Temperature- and Component-Dependent Degradation of Perovskite Photovoltaic Materials under Concentrated Sunlight. *J. Phys. Chem. Lett.* 2015, 6, 326−330.

(12) Li, W.; Li, J.; Wang, L.; Niu, G.; Gao, R.; Qiu, Y. Post Modification of Perovskite Sensitized Solar Cells by Aluminum Oxide for Enhanced Performance. *J. Mater. Chem. A* 2013, 1, 11735−11740.

(13) Li, M.; Li, H.; Fu, J.; Liang, T.; Ma, W. Recent Progress on the Stability of Perovskite Solar Cells in a Humid Environment. *J. Phys. Chem. C* 2020, 124, 27251−27266.

(14) Wu, X.; Trinh, M. T.; Niesner, D.; Zhu, H.; Norman, Z.; Owen, J. S.; Yaffe, O.; Kudisch, B. J.; Zhu, X.-Y. Trap States in Lead Iodide Perovskites. *J. Am. Chem. Soc.* 2015, 137, 2089−2096.

(15) Chen, Q.; De Marco, N.; Yang, Y.; Song, T.-B.; Chen, C.-C.; Zhao, H.; Hong, Z.; Zhou, H.; Yang, Y. Under the Spotlight: The Organic−Inorganic Hybrid Halide Perovskite for Optoelectronic Applications. *Nano Today* 2015, 10, 355−396.

(16) Kulbak, M.; Gupta, S.; Kedem, N.; Levine, I.; Bendikov, T.; Hodes, G.; Cahen, D. Cesium Enhances Long-Term Stability of Lead Bromide Perovskite-Based Solar Cells. *J. Phys. Chem. Lett.* 2016, 7, 167−172.

(17) López, C. A.; Martínez-Huerta, M. V.; Alvarez-Galván, M. C.; Kayser, P.; Gant, P.; Castellanos-Gomez, A.; Fernández-Díaz, M. T.; Fauth, F.; Alonso, J. A. Elucidating the Methylammonium (MA) Conformation in MAPbBr$_3$ Perovskite with Application in Solar Cells. *Inorg. Chem.* 2017, 56, 14214−14219.

(18) Yu, Z.; Leilaeioun, M.; Holman, Z. Selecting Tandem Partners for Silicon Solar Cells. *Nat. Energy* 2016, 1, 16137.

(19) Leijtens, T.; Bush, K. A.; Prasanna, R.; McGehee, M. D. Opportunities and Challenges for Tandem Solar Cells Using Metal Halide Perovskite Semiconductors. *Nat. Energy* 2018, 3, 828−838.

(20) Xu, J.; Boyd, C. C.; Yu, Z. J.; Palmstrom, A. F.; Witter, D. J.; Larson, B. W.; France, R. M.; Werner, J.; Harvey, S. P.; Wolf, E. J.; Weigand, W.; Manzoor, S.; van Hest, M. F. A. M.; Berry, J. J.; Luther, J. M.; Holman, Z. C.; McGehee, M. D. Triple-Halide Wide-Band Gap Perovskites with Suppressed Phase Segregation for Efficient Tandems. *Science* 2020, 367, 1097−1104.

(21) Manser, J. S.; Kamat, P. V. Band Filling with Free Charge Carriers in Organometal Halide Perovskites. *Nat. Photonics* 2014, 8, 737−743.

(22) Yang, Y.; Ostrowski, D. P.; France, R. M.; Zhu, K.; van de Lagemaat, J.; Luther, J. M.; Beard, M. C. Observation of a Hot-Phonon Bottleneck in Lead-Iodide Perovskites. *Nat. Photonics* 2016, 10, 53−59.

(23) Herz, L. M. Charge-Carrier Dynamics in Organic-Inorganic Metal Halide Perovskites. *Annu. Rev. Phys. Chem.* 2016, 67, 65−89.

(24) Stamplecoskie, K. G.; Manser, J. S.; Kamat, P. V. Dual Nature of the Excited State in Organic−Inorganic Lead Halide Perovskites. *Energy Environ. Sci.* 2015, 8, 208−215.

(25) Price, M. B.; Butkus, J.; Jellicoe, T. C.; Sadhanala, A.; Briane, A.; Halpert, J. E.; Broch, K.; Hodgkiss, J. M.; Friend, R. H.; Deschler, F. Hot-Carrier Cooling and Photoinduced Refractive Index Changes in Organic−Inorganic Lead Halide Perovskites. *Nat. Commun.* 2015, 6, 8420.

(26) Yang, J.; Wen, X.; Xia, H.; Sheng, R.; Ma, Q.; Kim, J.; Tapping, P.; Harada, T.; Kee, T. W.; Huang, F.; Cheng, Y.-B.; Green, M.; Ho-Baillie, A.; Huang, S.; Shrestha, S.; Patterson, R.; Conibeer, G. Acoustic-Optical Phonon up-Conversion and Hot-Phonon Bottleneck in Lead-Halide Perovskites. *Nat. Commun.* 2017, 8, 14120.

(27) Xing, G.; Mathews, N.; Sun, S.; Lim, S. S.; Lam, Y. M.; Grätzel, M.; Mhaisalkar, S.; Sum, T. C. Long-Range Balanced Electron- and Hole-Transport Lengths in Organic-Inorganic CH$_3$NH$_3$PbI$_3$. *Science* 2013, 342, 344−347.

(28) Shi, J.; Li, Y.; Li, Y.; Li, D.; Luo, Y.; Wu, H.; Meng, Q. From Ultrafast to Ultraslow: Charge-Carrier Dynamics of Perovskite Solar Cells. *Joule* 2018, 2, 879−901.

(29) deQuilettes, D. W.; Frohna, K.; Emin, D.; Kirchartz, T.; Bulovic, V.; Ginger, D. S.; Stranks, S. D. Charge-Carrier Recombination in Halide Perovskites. *Chem. Rev.* 2019, 119, 11007−11019.

(30) Li, C.; Wang, A.; Deng, X.; Wang, S.; Yuan, Y.; Ding, L.; Hao, F. Insights into Ultrafast Carrier Dynamics in Perovskite Thin Films and Solar Cells. *ACS Photonics* 2020, 7, 1893−1907.

(31) Elshanawany, M. M.; Ricciardulli, A. G.; Saliba, M.; Wachtveitl, J.; Braun, M. Mechanism of Ultrafast Energy Transfer between the Organic−Inorganic Layers in Multiple-Ring Aromatic Spacers for 2D Perovskites. *Nanoscale* 2021, 13, 15668−15676.

(32) Ghosh, T.; Aharon, S.; Etgar, L.; Ruhman, S. Free Carrier Emergence and Onset of Electron−Phonon Coupling in Methyl-

ammonium Lead Halide Perovskite Films. *J. Am. Chem. Soc.* **2017**, *139*, 18262−18270.

(33) Miyata, K.; Meggiolaro, D.; Trinh, M. T.; Joshi, P. P.; Mosconi, E.; Jones, S. C.; De Angelis, F.; Zhu, X.-Y. Large Polarons in Lead Halide Perovskites. *Sci. Adv.* **2017**, *3*, No. e1701217.

(34) Kahmann, S.; Loi, M. A. Hot Carrier Solar Cells and the Potential of Perovskites for Breaking the Shockley−Queisser Limit. *J. Mater. Chem. C* **2019**, *7*, 2471−2486.

(35) Minda, I.; Horn, J.; Ahmed, E.; Schlettwein, D.; Schwoerer, H. Ultrafast Charge Dynamics in Mixed Cation − Mixed Halide Perovskite Thin Films. *ChemPhysChem* **2018**, *19*, 3010−3017.

(36) Tan, H.; Che, F.; Wei, M.; Zhao, Y.; Saidaminov, M. I.; Todorović, P.; Broberg, D.; Walters, G.; Tan, F.; Zhuang, T.; Sun, B.; Liang, Z.; Yuan, H.; Fron, E.; Kim, J.; Yang, Z.; Voznyy, O.; Asta, M.; Sargent, E. H. Dipolar Cations Confer Defect Tolerance in Wide-Bandgap Metal Halide Perovskites. *Nat. Commun.* **2018**, *9*, 3100.

(37) Saidaminov, M. I.; Williams, K.; Wei, M.; Johnston, A.; Quintero-Bermudez, R.; Vafaie, M.; Pina, J. M.; Proppe, A. H.; Hou, Y.; Walters, G.; Kelley, S. O.; Tisdale, W. A.; Sargent, E. H. Multi-Cation Perovskites Prevent Carrier Reflection from Grain Surfaces. *Nat. Mater.* **2020**, *19*, 412−418.

(38) Gélvez-Rueda, M. C.; Van Gompel, W. T. M.; Herckens, R.; Lutsen, L.; Vanderzande, D.; Grozema, F. C. Inducing Charge Separation in Solid-State Two-Dimensional Hybrid Perovskites through the Incorporation of Organic Charge-Transfer Complexes. *J. Phys. Chem. Lett.* **2020**, *11*, 824−830.

(39) Brauer, J. C.; Tsokkou, D.; Sanchez, S.; Droseros, N.; Roose, B.; Mosconi, E.; Hua, X.; Stolterfoht, M.; Neher, D.; Steiner, U.; De Angelis, F.; Abate, A.; Banerji, N. Comparing the Excited-State Properties of a Mixed-Cation−Mixed-Halide Perovskite to Methyl-ammonium Lead Iodide. *J. Chem. Phys.* **2020**, *152*, 104703.

(40) Baumeler, T.; Arora, N.; Hinderhofer, A.; Akin, S.; Greco, A.; Abdi-Jalebi, M.; Shivanna, R.; Uchida, R.; Liu, Y.; Schreiber, F.; Zakeeruddin, S. M.; Friend, R. H.; Graetzel, M.; Dar, M. I. Minimizing the Trade-Off between Photocurrent and Photovoltage in Triple-Cation Mixed-Halide Perovskite Solar Cells. *J. Phys. Chem. Lett.* **2020**, *11*, 10188−10195.

(41) Pasanen, H. P.; Vivo, P.; Canil, L.; Hempel, H.; Unold, T.; Abate, A.; Tkachenko, N. V. Monitoring Charge Carrier Diffusion across a Perovskite Film with Transient Absorption Spectroscopy. *J. Phys. Chem. Lett.* **2020**, *11*, 445−450.

(42) Wang, T.; Jin, L.; Hidalgo, J.; Chu, W.; Snaider, J. M.; Deng, S.; Zhu, T.; Lai, B.; Prezhdo, O.; Correa-Baena, J.-P.; Huang, L. Protecting Hot Carriers by Tuning Hybrid Perovskite Structures with Alkali Cations. *Sci. Adv.* **2020**, *6*, No. eabb1336.

(43) Catone, D.; Ammirati, G.; O'Keeffe, P.; Martelli, F.; Di Mario, L.; Turchini, S.; Paladini, A.; Toschi, F.; Agresti, A.; Pescetelli, S.; Di Carlo, A. Effects of Crystal Morphology on the Hot-Carrier Dynamics in Mixed-Cation Hybrid Lead Halide Perovskites. *Energies* **2021**, *14*, 708.

(44) Saliba, M.; Correa-Baena, J.-P.; Wolff, C. M.; Stolterfoht, M.; Phung, N.; Albrecht, S.; Neher, D.; Abate, A. How to Make over 20% Efficient Perovskite Solar Cells in Regular (n−i−p) and Inverted (p−i−n) Architectures. *Chem. Mater.* **2018**, *30*, 4193−4201.

(45) Reuss, A. J.; Grünewald, C.; Braun, M.; Engels, J. W.; Wachtveitl, J. The Three Possible 2-(Pyrenylethynyl) Adenosines: Rotameric Energy Barriers Govern the Photodynamics of These Structural Isomers. *ChemPhysChem* **2016**, *17*, 1369−1376.

(46) Gustmann, H.; Lefrancois, D.; Reuss, A. J.; Gophane, D. B.; Braun, M.; Dreuw, A.; Sigurdsson, S. T.; Wachtveitl, J. Spin the Light off: Rapid Internal Conversion into a Dark Doublet State Quenches the Fluorescence of an RNA Spin Label. *Phys. Chem. Chem. Phys.* **2017**, *19*, 26255−26264.

(47) Trojanowski, P.; Plötner, J.; Grünewald, C.; Graupner, F. F.; Slavov, C.; Reuss, A. J.; Braun, M.; Engels, J. W.; Wachtveitl, J. Photo-Physical Properties of 2-(1-Ethynylpyrene)-Adenosine: Influence of Hydrogen Bonding on Excited State Properties. *Phys. Chem. Chem. Phys.* **2014**, *16*, 13875−13888.

(48) Slavov, C.; Hartmann, H.; Wachtveitl, J. Implementation and Evaluation of Data Analysis Strategies for Time-Resolved Optical Spectroscopy. *Anal. Chem.* **2015**, *87*, 2328−2336.

(49) Mondal, N.; Samanta, A. Complete Ultrafast Charge Carrier Dynamics in Photo-Excited All-Inorganic Perovskite Nanocrystals ($CsPbX_3$). *Nanoscale* **2017**, *9*, 1878−1885.

(50) Trinh, M. T.; Wu, X.; Niesner, D.; Zhu, X.-Y. Many-Body Interactions in Photo-Excited Lead Iodide Perovskite. *J. Mater. Chem. A* **2015**, *3*, 9285−9290.

(51) Chen, J.; Messing, M. E.; Zheng, K.; Pullerits, T. Cation-Dependent Hot Carrier Cooling in Halide Perovskite Nanocrystals. *J. Am. Chem. Soc.* **2019**, *141*, 3532−3540.

(52) Chen, K.; Barker, A. J.; Morgan, F. L. C.; Halpert, J. E.; Hodgkiss, J. M. Effect of Carrier Thermalization Dynamics on Light Emission and Amplification in Organometal Halide Perovskites. *J. Phys. Chem. Lett.* **2015**, *6*, 153−158.